Forest Ecology and Management 393 (2017) 63–73

Contents lists available at ScienceDirect

Forest Ecology and Management

journal homepage: www.elsevier.com/locate/foreco

Characterizing degradation of palm swamp peatlands from space and on the ground: An exploratory study in the Peruvian Amazon

Kristell Hergoualc'h [a,*], Victor Hugo Gutiérrez-Vélez [a,b], Mary Menton [a], Louis V. Verchot [a,c]

[a] Center for International Forestry Research (CIFOR), Jl. CIFOR, Situ Gede, Bogor 16115, Indonesia
[b] Temple University, Department of Geography and Urban Studies, 321 Gladfelter Hall, 1115 W. Berks Street, Philadelphia, PA 19122, USA
[c] Center for International Tropical Agriculture (CIAT), Km 17, Recta Cali-Palmira, Cali, Colombia

ARTICLE INFO

Article history:
Received 4 October 2016
Accepted 12 March 2017

Keywords:
Aguajal
CO_2
Mauritia flexuosa
Tropical peatland
Land cover classification
Remote sensing
Satellite data

ABSTRACT

Peru has the fourth largest area of peatlands in the Tropics. Its most representative land cover on peat is a *Mauritia flexuosa* dominated palm swamp (thereafter called dense PS), which has been under human pressure over decades due to the high demand for the *M. flexuosa* fruit often collected by cutting down the entire palm. Degradation of these carbon dense forests can substantially affect emissions of greenhouse gases and contribute to climate change. The first objective of this research was to assess the impact of dense PS degradation on forest structure and biomass carbon stocks. The second one was to explore the potential of mapping the distribution of dense PS with different degradation levels using remote sensing data and methods. Biomass stocks were measured in 0.25 ha plots established in areas of dense PS with low (n = 2 plots), medium (n = 2) and high degradation (n = 4). We combined field and remote sensing data from the satellites Landsat TM and ALOS/PALSAR to discriminate between areas typifying dense PS with low, medium and high degradation and *terra firme*, *restinga* and mixed PS (not *M. flexuosa* dominated) forests. For this we used a Random Forest machine learning classification algorithm. Results suggest a shift in forest composition from palm to woody tree dominated forest following degradation. We also found that human intervention in dense PS translates into significant reductions in tree carbon stocks with initial (above and below-ground) biomass stocks (135.4 ± 4.8 Mg C ha^{-1}) decreased by 11 and 17% following medium and high degradation. The remote sensing analysis indicates a high separability between dense PS with low degradation from all other categories. Dense PS with medium and high degradation were highly separable from most categories except for *restinga* forests and mixed PS. Results also showed that data from both active and passive remote sensing sensors are important for the mapping of dense PS degradation. Overall land cover classification accuracy was high (91%). Results from this pilot analysis are encouraging to further explore the use of remote sensing data and methods for monitoring dense PS degradation at broader scales in the Peruvian Amazon. Providing precise estimates on the spatial extent of dense PS degradation and on biomass and peat derived emissions is required for assessing national emissions from forest degradation in Peru and is essential for supporting initiatives aiming at reducing degradation activities.

1. Introduction

Peatlands store large amounts of carbon (C) in their soil. According to recent estimates, the C stored in global tropical peat soils is equivalent to about 40% of the total C stored in woody vegetation in the entire tropics (Page et al., 2011; Baccini et al., 2012). The luxuriant tropical rainforests living on rich C deposits also store substantial amounts of C in their biomass. (Murdiyarso et al., 2009). Tropical peatlands are estimated to cover an area between 368,500 and 441,025 km^2 representing 8–11% of global peatland area (Yu et al., 2010; Page et al., 2011). Indonesia, Democratic Republic of Congo, Northern Republic of Congo and Peru are the countries with the largest areas of peatland in the tropics (Page et al., 2011; Dargie et al., 2017). Peru harbors lowland peatlands in the Amazon basin as well as highland peatlands in the Andes (Román-Cuesta et al., 2011; Draper et al., 2014). In lowlands, Draper et al. (2014) estimated peatland areas of 35,600 km^2 in the Pastaza-Marañon basin and Householder et al. (2012) 294 km^2 in the floodplain of the river Madre de Dios; for a total of 35,894 km^2.

* Corresponding author at: CIFOR, c/o Centro Internacional de la Papa (CIP), Av. La Molina 1895, La Molina, Apdo postal 1558, 15024 Lima, Peru.
E-mail address: k.hergoualch@cgiar.org (K. Hergoualc'h).

http://dx.doi.org/10.1016/j.foreco.2017.03.016
0378-1127/

While in Indonesia the majority of peatlands are ombrotrophic domes (Jaenicke et al., 2008) supporting the growth of a variety of swamp forest types (Brady, 1997; Laumonier, 1997), both minerotrophic and ombrotrophic peatlands are found in the Peruvian Amazon basin. The distinction between minerotrophic and ombrotrophic environments is based on the origin of water and nutrient supply; from streams and ground-water in the first case, from precipitation in the second one. The different water regimes and associated nutrient status led to a diversity of ecosystem types: pole forest peatlands, palm swamp peatlands (locally known as 'aguajales') and opened peatlands made up of herbaceous communities with or without dispersed palms (Lähteenoja et al., 2009a; Lähteenoja and Roucoux, 2010; Lähteenoja and Page, 2011; Householder et al., 2012). Pole forests were described by Draper et al. (2014) and Kelly et al. (2014) as being low stature with thin-stemmed trees and excluding many species. Palm swamps (PS) are the main peatland ecosystem type in the Peruvian Amazon basin (Draper et al., 2014). These palm dominated forests are classified as dense and mixed PS (IIAP, 2004; Freitas et al., 2006; González-B. and Rial, 2013). Dense PS formations are permanently flooded depressions which lie parallel to the river bed between ridges. The substratum is clayey, and retains rainfall. River water enters the depressions only at the time of highest flooding (Kahn and Mejia, 1990). Dense PS are dominated by the *Mauritia flexuosa* (or 'aguaje') palm. Mixed PS are partially exposed to seasonal flooding of nearby rivers (IIAP, 2004). Unlike dense PS, mixed PS are not dominated by *M. flexuosa*, they are formed by communities of *M. flexuosa* associated with other palms or trees (*Ficus* sp. or *Coussapoa* sp.). Permanently flooded dense PS seem to grow on peat soil exclusively whereas seasonally flooded mixed PS are observed to grow both on peat (Freitas et al., 2006) and mineral soils (this study, and field observations).

Tropical peatlands are subject to increasing pressures that threaten the stability of the stored C pools, especially in Indonesia where large amounts of greenhouse gases (GHG) have been released as a consequence mainly of agricultural expansion and fires (van der Werf et al., 2008; Koh et al., 2011; Gaveau et al., 2014; Hergoualc'h and Verchot, 2014). Peruvian lowland peatlands are found to be under less pressure than Indonesian ones although logging, oil and gas prospection, gold mining, agriculture, grazing and settlements are becoming increasingly frequent (Lähteenoja et al., 2012; Janovec et al., 2013). Peatlands in tropical montane cloud forests in the Peruvian Andes have also been shown to experience extensive fire pressure (Román-Cuesta et al., 2011). PS have been the subject of heavy degradation over the past decades due to the high local and regional demand for the *M. flexuosa* fruit and the 'suri' larva, which grows inside the trunk of dead palms and is an important source of protein for rural residents (Padoch, 1988; Penn, 2008; Horn et al., 2012). Despite the existence of viable sustainable harvesting techniques, the collection of *M. flexuosa* fruits is extensively performed by cutting the entire palm (Appendix 1). This degradation of PS compromises the renewal of *M. flexuosa* populations and causes genetic degradation because *M. flexuosa* extractors usually select the females with the best quality and biggest fructifications (Penn, 2008). Degradation leads to a change in the sex ratio of palms with a decrease in female densities (Horn et al., 2012); it also constitutes a threat to a variety of mammal species that depend on them (Penn, 2008).

Forest degradation can contribute substantially to national emissions however these emissions are generally disregarded as they are more technically challenging to measure than emissions from deforestation (Pearson et al., 2017). The use of satellite data for monitoring degradation implies identifying often-subtle differences in reflectance between conserved and degraded forest. In addition degradation patches are generally small compared with clearings which difficults their identification (Miettinen et al., 2014; Shimabukuro et al., 2014).

Remote sensing efforts on peatlands in the Peruvian Amazon include the work by Lähteenoja et al. (2012) who developed a map discriminating different types of peatland forests, wetlands and other land covers in the Pastaza-Marañon basin through an unspecified supervised classification of Landsat images based on field observations. However no classification accuracy assessment was performed. More recently, Draper et al. (2014) used data from the satellite sensors Landsat, ALOS-PALSAR and SRTM along with ground referencing points of known classes to map the spatial distribution of peatlands also in the Pastaza-Marañon foreland. Classification was performed using a supervised, support vector machine method. Land cover classes considered were pole forests, PS and open peatlands as well as four non peat-forming categories (*terra firme* forests or occasionally flooded forests, seasonally flooded forests, open water and urban areas). The overall classification accuracy was 95%.

Attempts at mapping peat forest degradation has been limited to Indonesia. Miettinen et al. (2012), Miettinen and Liew (2010a) and Miettinen and Liew (2010b) visually interpreted time series of optical data from Landsat and SPOT satellites to assess degradation in Sumatra and Kalimantan. Hereafter, Englhart et al. (2013) combined optical and lidar data to assess changes in aboveground biomass between 2007 and 2011 in central Kalimantan. Medium and high resolution data from Landsat and RapidEye sensors were used to identify unaffected, selectively logged, and burned forests while lidar data were correlated with field biomass measurements.

Despite the importance of accounting greenhouse gas emissions from forest degradation, very limited monitoring or research has been conducted on degradation of Peruvian lowland peatlands. In particular there is to date no assessment on the impact that over-harvesting of *M. flexuosa* in dense PS can have on forest structure and functions. Previous attempts to classify and map peatland ecosystems in the Peruvian Amazon (Lähteenoja et al., 2012; Draper et al., 2014) have set aside past and on-going degradation activities in dense PS. To evaluate and map the extent of degradation it is essential to develop new methods suitable for dense PS. With this work we intend to provide a first and preliminary quantification of the impact of dense PS degradation on forest structure, composition and biomass C stocks. We also explore the potential of remote sensing data from the satellites Landsat and ALOS-PALSAR to distinguish areas of dense PS from other land covers and to further discriminate these areas under different levels of degradation using satellite and field data from one single year.

2. Materials and methods

2.1. Study area

The case study was conducted in the Peruvian Amazon, Region of *Loreto*, in the watersheds of the *Marañon* and *Ucayali* rivers (Fig. 1). The site is located 90–130 m above sea level and has mean annual air temperature and precipitation of 26 °C and 3100 mm. The study encompassed an area of 351,324 ha which included the *Pacaya-Samiria* National reserve in the *Yanayacu-Pucate* watershed. This watershed is part of the *Pastaza-Marañon* basin, the most extensive continuous wetland area of the Peruvian Amazon (Räsänen et al., 1992). The selected area offered the opportunity to measure dense PS with different levels of degradation from low and medium degradation inside the *Pacaya-Samiria* reserve (Gonzales Davila et al., 2007) to high degradation outside the reserve, in particular near the *Tigre* river where *M. flexuosa* fruit has been extracted intensively since the 80s (Padoch, 1988; Penn et al., 2008).

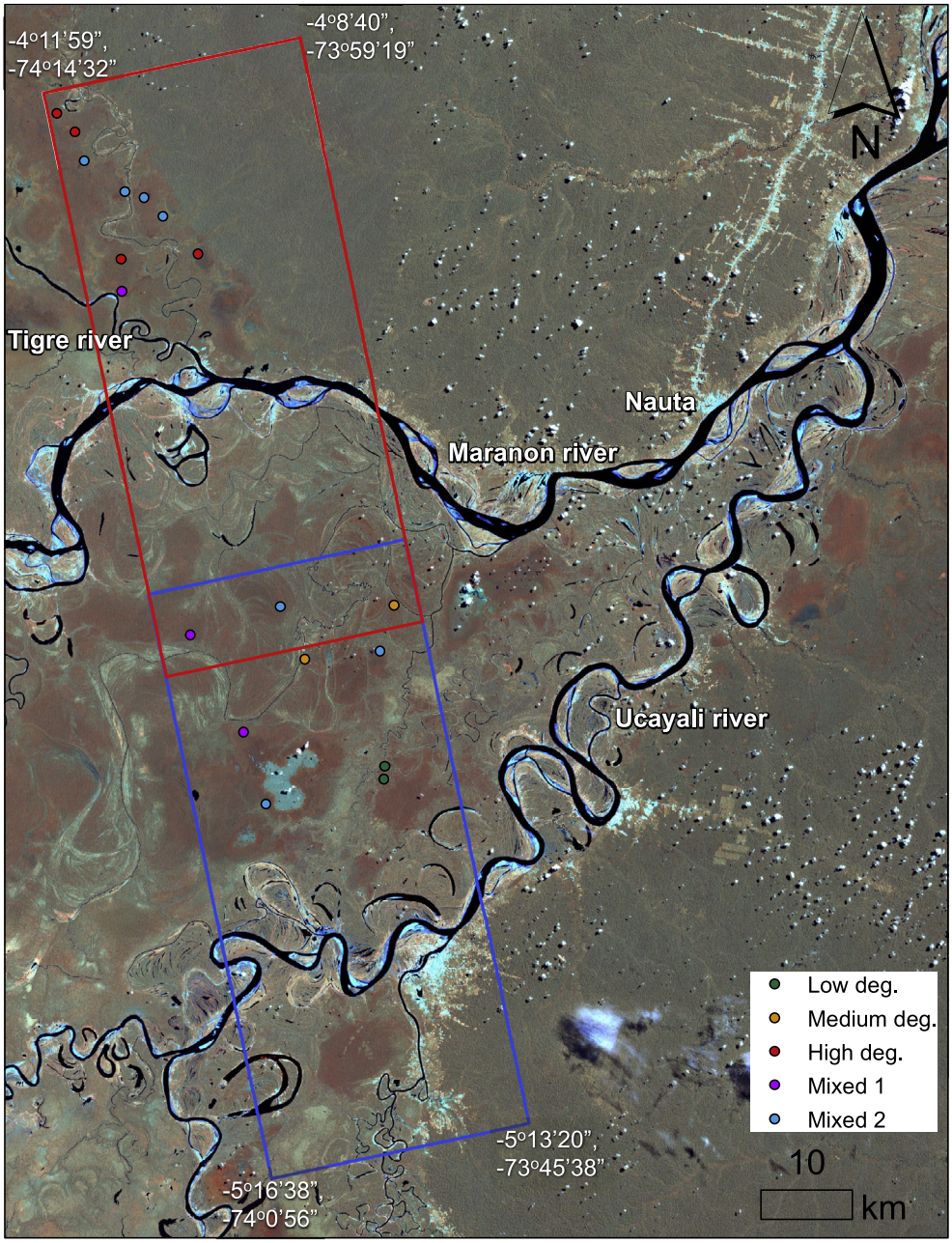

Fig. 1. Location of the study area. The sampling area is represented by the extent enclosed by the blue and red frames which correspond to the two ALOS-PALSAR scenes that were used in the remote sensing analysis (Table 1). The background consists of a red, green, blue satellite composite using bands 4, 5 and 7 from the two Landsat scenes used in the analysis. A 2.5 standard deviation stretch was applied to the composite to improve visualization. Symbols represent the location of the sites visited in the field. Coordinates represent the geographic corners of the study area. (For interpretation of the references to colour in this figure legend, the reader is referred to the web version of this article.)

2.2. Field data collection, processing and biomass estimation

Field survey consisted of the measurement of forest plots representing different levels of degradation in dense PS. The campaign included also the collection of field data to assess the suitability to differentiate associations of dense PS from other forest types using remote sensing data. The fieldwork was carried out during five weeks starting on January 29th 2013.

Prior to the establishment of plots, we pre-selected candidate areas with a high chance of including dense PS associations with different levels of degradation based on the visual interpretation of Landsat reflectance data and pre-measurement informal conversations with *M. flexuosa* extractors in the zone. Visual interpretation was performed by creating red, green, blue composites with bands 4, 5 and 7 of Landsat images from the year 2011 (Table 1). This band combination has proved to be suitable for localizing wetlands (Lähteenoja et al., 2009b). Candidate areas were identified based on the following criteria: (1) The area should correspond to a dense PS association representing different levels of degradation; (2) Accessibility to the area should be reasonable to allow time for performing the measurements; and (3) The sampling area should typify a level of degradation of an extent of at least 5 ha to

Table 1
Geographic data sources used for the analysis.

Data	Date	Number of scenes	Granule ID path/row	Format	Spatial resolution	Source
Landsat TM	09/07/2011, 09/15/2011	4	06–07, 063–064	Raster	30 m	GLOVIS (2013)
ALOS PALSAR	04/02/2011	2	ALPSRP276287090, ALPSRP2762870100	Raster	12.5 m	PASCO (2013)
Digital elevation model	02/11/2000	2	S05-06 W074-075	Raster	3 arc sec	Earth explorer (2013)
Rivers	2006	–	–	Vector	–	Lehner et al. (2006)

reduce the likelihood of mixing spectral information from surrounding areas with different levels of degradation or other land covers in the remote sensing analysis.

Due to resource, time and access constraints, we set as an objective to sample 2–3 plots per strata (low, medium, high degradation). Given the small sample size, we opted for an opportunistic site selection approach rather than a random or a systematic one. A total of twenty sites were visited. The sites were inspected and their coordinates collected using a hand held GPS with a precision of 3 m. The coordinates were taken in a point around which the land cover condition was homogenous over a distance of at least 100 m. Twelve of the visited sites corresponded to mixed PS. The rest were dense PS growing on peat. The soil was characterized as peat or non-peat visually (dark brown to black color) and olfactorily (organic odor). The degradation level of the eight dense PS was assessed according to local knowledge by *M. flexuosa* harvesters about historic practices such as intensity and method of fruit extraction (palm cutting versus climbing) and structural characteristics of the visited forest areas. Degradation was characterized in three levels as:

- Low: defined as undisturbed areas and identified by communities as being not harvested, with absence of stumps or other signs of tree-cutting.
- Moderate: defined as disturbed areas and identified by communities as being actively but moderately harvested, with presence of cut palms or other degradation evidence.
- High: defined as disturbed areas and identified by communities as being actively harvested intensively and for decades, with presence of cut palms or other degradation evidence.

Two of the dense PS were identified as exhibiting low degradation, two as being moderately degraded and the other four were highly degraded lands.

Biomass plots were established in the eight dense PS. The centroid of the measurement plot was previously identified on a map and the center of the plot was located at <50 m from the targeted point. Then we set up square plots of 50×50 m (2500 m^2). This area size was chosen as a good compromise between intra-plot spatial variability and sampling efficiency in flooded conditions. The plot was divided into four 25×25 m subplots that were measured independently. We also established miniplots of 10×10 m (100 m^2) in each one of the corners of the plot area to measure smaller trees. In each of the 25×25 m subplots, we measured the diameter at breast height (DBH) of all trees with a DBH >10 cm using a diameter tape and the height (H) of all palms taller than 3 m with a clinometer. The height of the palms was measured from the ground to the highest point of the highest leaf. In the 10×10 m miniplots, we measured the DBH of all trees with a DBH between 2.5 and 10 cm with a caliper and the H of palms between 1 and 3 m tall with a graduated stick. The height for measuring diameter in atypical trees was located using the CFE (Centre for Standardization and Environment, 2011) standards. All DBH and H measurements, most vernacular name of trees and palms and number of stumps in each subplot were recorded.

Tree biomass was predicted from H for palms or from DBH for woody trees using allometric equations (Table 2). Equations to predict above and belowground biomass as a function of H for *M. flexuosa* and *Mauritiella armata* ('aguajillo') were fitted to the data reported by Freitas et al. (2006) (Appendix 2). We applied a Chapman-Richards equation form (Weiskittel et al., 2011) for aboveground biomass in *M. flexuosa* to not over-estimate biomass in tall palms; otherwise we fitted linear regressions using either H or its logarithm and the logarithm of biomass to facilitate model fitting and reduce heteroscedasticity. We used the same equation developed for *M. armata* to estimate belowground biomass in other palms, assuming that they follow a similar relationship. Aboveground biomass of woody trees was computed from a model which has proved to simulate with little bias biomass of moist forest in the Colombian Amazon (Alvarez et al., 2012). The height of woody trees was calculated from the DBH. Carbon stock in biomass was calculated applying a carbon fraction in dry matter of 48% (IPCC, 2006; Goodman et al., 2013).

Table 2
Equations used for predicting biomass for individual trees.

Species	Equation	R^2 (%)	Source
M. flexuosa	$AGB = 1412.71 \times (1 - e^{-0.092H})^{5.93}$	–[a]	–[b]
	$Ln(BGB) = -3.29 + 2.73 \times Ln(H)$	98	–[b]
M. armata	$Ln(AGB) = -0.07 + 1.32 \times Ln(H)$	92	–[b]
	$Ln(BGB) = 0.64 + 0.12 \times H$	100	–[b]
Other palms	$Ln(AGB) = 0.360 + 1.218 \times Ln(H)$	65	Sierra et al. (2007)
	BGB see *M. armata*		
Woody trees	$AGB = 0.1424 \times DBH^{2.3679}$	n.a.	Zianis (2008)
	$BGB = 0.205 \times AGB$	n.a.	Mokany et al. (2006)[c]
	$Ln(H) = 0.893 - E + 0.760 \times Ln(DBH) - 0.0340 \times [Ln(DBH)]^2$	n.a.	Chave et al. (2014)

AGB (kg d.m. $tree^{-1}$): aboveground biomass, *BGB* (kg d.m. $tree^{-1}$): belowground biomass, *H*: tree height (m), *DBH*: diameter at breast height (cm), E: measure of environmental stress (−0.045 in the present case), n.a. not available.

[a] R^2 was not calculated because it is not a suitable indicator of fitness for non-linear regressions.

[b] Here with data from Freitas et al. (2006). The parameters for evaluating the goodness of fit and predictability of the models are presented in Appendix 2.

[c] Tropical moist forest for shoot biomass <125 Mg dm ha^{-1}.

2.3. Satellite analysis

We used Landsat images for pre-survey inspections in peatland areas and combined them with ALOS-PALSAR data to evaluate the ability to discriminate areas of dense PS from other types of vegetation and to map their degradation (Table 1, Appendix 3). The ALOS-PALSAR images corresponded to quad-polarization mode (HH, HV, VH, VV) and were acquired at 1.5 processing level. This is a multi-look-processed image with fine-beam single polarization mode and a native resolution of 12.5 m. We selected ALOS-PALSAR information because of its sensitivity to structural changes that can provide complementary information to the spectral data from Landsat (Saatchi et al., 2011). Landsat TM images were downloaded at level-1 processing level (radiometrically calibrated and geometrically corrected). Pre-processing of the Landsat images was performed following the procedure used by Gutiérrez-Vélez and DeFries (2013) and consisted first of the transformation of digital numbers into reflectance (Chander et al., 2009). Then the images were radiometrically normalized using pseudo-invariant features. Pseudo invariant features were selected by applying a multi-band statistical analysis of the distribution of the difference in reflectance in each band between two images. Pixels with a sum of the standardized squares of the difference in reflectance below a defined threshold were considered pseudo-invariant. The threshold was defined assuming a chi-square distribution with a probability level of 99.9%. Radiometric normalization was applied given the differences in acquisition dates between the two paths of Landsat scenes used in the images. This allowed to reduce dissimilarities between the two images caused by differences in acquisition conditions including sensor performance, solar irradiance and atmospheric conditions (Yuan and Elvidge, 1996). Therefore atmospheric correction was not necessary. Finally we performed a tasseled cap transformation to the Landsat image to reduce the dimensionality of Landsat data and maximize the sensitivity to biophysical parameters of interest while reducing internal and external effect (Jensen, 2016). The tasseled cap bands correspond to brightness, greenness and third. The coefficients used to obtain the tasseled cap components are the ones incorporated in the software ENVI which were derived from Crist and Cicone (1984). The component named "third" relates to soil features, including soil moisture and was named as such by the above-mentioned authors. Pre-processing of the radar images consisted of the conversion of digital numbers into power values. Geometric and radiometric corrections were applied to the images using inputs from a Digital Elevation Model at a 3 arc second resolution using the forward geocoding approach (ASF, 2013). Then the images were co-registered using the Landsat images as reference with a root mean square error <0.5 pixels. Finally, a 3×3 Frost smoothing filter was applied to the radar satellite images to reduce speckle. The Frost filter has demonstrated a better performance than other filters at preserving edges, linear features and target information for land cover classification (Nyoungui et al., 2002). Therefore it was deemed suitable for this work. Before conducting the satellite analysis, we created a geographic database containing polygons representing a buffered area of 60 m around the center point of the sampled areas. This buffer was selected to include pixels representing the local spectral variability of the sampled points. A tabular database was also created with the structural data of the polygon associated with each plot and it was linked to their respective geographic information.

To test the suitability for discriminating dense PS from other land covers, we referenced in the field the location of areas representing the most typical vegetation types in the zone. These land covers included *terra firme*, *restinga* forests and areas of mixed PS. *Terra firme* forests are located in non-flooded areas. *Restinga* forests occur on periodically flooded alluvial soils and are dominated by woody tree species. Mixed PS are seasonally flooded forests with *M. flexuosa* communities associated with other palms or trees (IIAP, 2004). Training data from *terra firme* and *restinga* forests were collected visually using a false composite with Landsat bands 4, 5 and 7. Differences between non-flooded and flooded forests are visually conspicuous when using this band combination (Lähteenoja et al., 2009b; Lähteenoja et al., 2012). Differences between dense and mixed PS were less conspicuous visually. Therefore we collected additional ground data from visited mixed PS in the field to assess the ability to discriminate them from dense PS. We further discriminated mixed PS in two separate classes because the training polygons associated with this land cover formed two very distinct groups in the spectral space (Appendix 4). Other land covers included barren lands predominately composed by sand deposits along rivers, lakes, and converted areas.

The spectral space associated with data collected for each type of vegetation was visually explored using the n-D visualizer tool in ENVI to identify the most sensitive bands for differentiating land cover types. In addition, a quantitative separability analysis was performed, using the Jeffries-Matusita separability measure, to evaluate the ability of the bands to discriminate between pairs of land cover classes (Richards, 1999). Jeffries-Matusita values range between 0 and 2. Values >1.9 indicate that pairs of land cover classes are statistically separable. Values between 1 and 1.9 denote that the separability should be improved either by editing the training points or increasing the sample. Values <1 mean a poor separability and therefore that the compared land cover classes should be merged.

The spectral data for each land cover type was entered into a random forest classification algorithm to map the geographic distribution of dense PS under different levels of degradation, and discriminate them from other land covers. Random forest is a machine-learning algorithm that uses a bootstrapping approach to construct decision trees iteratively by splitting the data in two random sub-samples in each iteration. The first subsample is used for calibration and the other one for validation (Breiman, 2001). Therefore random forest does not require a set-aside data set to validate the classification. Random forest was used because it has demonstrated superior performance compared to other machine learning methods (Fernández-Delgado et al., 2014) and it has been widely adopted for remote sensing analysis (Belgiu and Drăguţ, 2016). To reduce biases in classification toward classes with the largest amount of training pixels, the training data were stratified and an equal amount of training pixels (27) from all land cover classes was selected randomly in each iteration (Appendix 5) (Gutiérrez-Vélez and DeFries, 2013). Accuracy for the land cover classification was expressed as producer's user's and overall accuracy. A post classification 3×3 majority filter was applied to the data to reduce speckle and other spurious artifacts. The importance of the different remote sensing variables for classification was obtained from two metrics obtained as part of the outputs of the remote sensing algorithm. The first one is the mean decrease in accuracy and is a measure of the reduction in accuracy if a given variable is removed from the classification. The second one is the mean decrease in Gini index, which is a measure of the power of each variable to split the training data into different training classes. Image processing was done using the ENVI 5.0.2 software (ITT, 2013) and the random forest algorithm was ran in the R statistical environment (R Core Team, 2013).

2.4. Statistics

Statistical analysis was performed using the software Infostat (2014), with a probability level of 5% to test the significance of degradation effects. The goodness of fit of the allometric models for calculating the biomass of *M. flexuosa* and *M. Armata* was

evaluated using the coefficient of determination (R^2, for linear models only) and residual standard error (RSE). Their predictability was assessed by average and standard deviation of the relative error (Goodman et al., 2013). The distribution of each variable was evaluated using the Shapiro–Wilk test. ANOVA and the non-parametric Kruskal–Wallis tests were performed for multiple comparisons when the residuals of the variables were normally and non-normally distributed. The average ± SE of tree density and biomass C stock were calculated from two replicate plots in low and medium degradation areas and four replicate plots in highly degraded dense PS.

3. Results and discussion

3.1. Forest structure and carbon stocks

The allometric models estimated accurately the above and below-ground biomass of *M. flexuosa* and *M. Armata* palms with standard errors of the bias in estimating biomass between 0.2 and 18% (Appendix 2) (Manuri et al., 2014). In total 2440 trees were measured across the eight dense PS plots. Results on structural variables indicate an increase in total tree density with degradation significant at the 0.1 level ($P = 0.09$) (Fig. 2 left). This

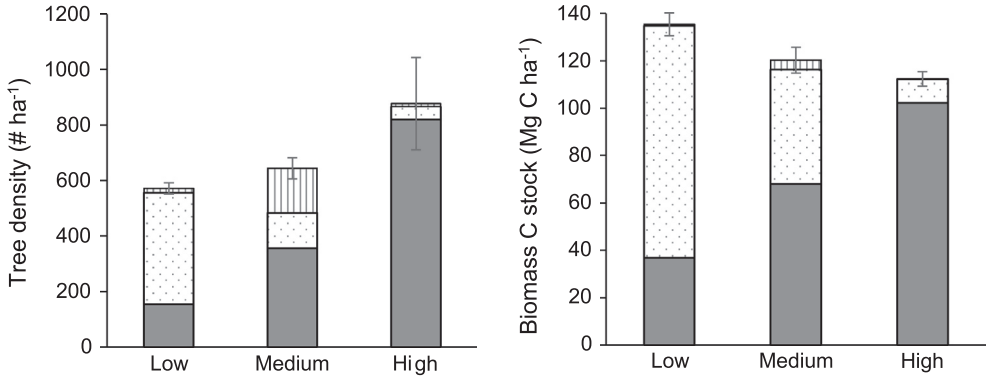

Fig. 2. Tree density (left) and biomass (above and below-ground) carbon stock (right) in dense palm swamp plots with different levels of degradation (low (n = 2), medium (n = 2), high (n = 4)). Solid grey, dot, and stripe fills indicate woody tree, *M. flexuosa* palm and other palms, respectively. The analysis considered woody trees with a DBH > 10 cm and palms with a H > 3 m. Error bars indicate the standard error associated to tree density and biomass carbon stock in each degradation level.

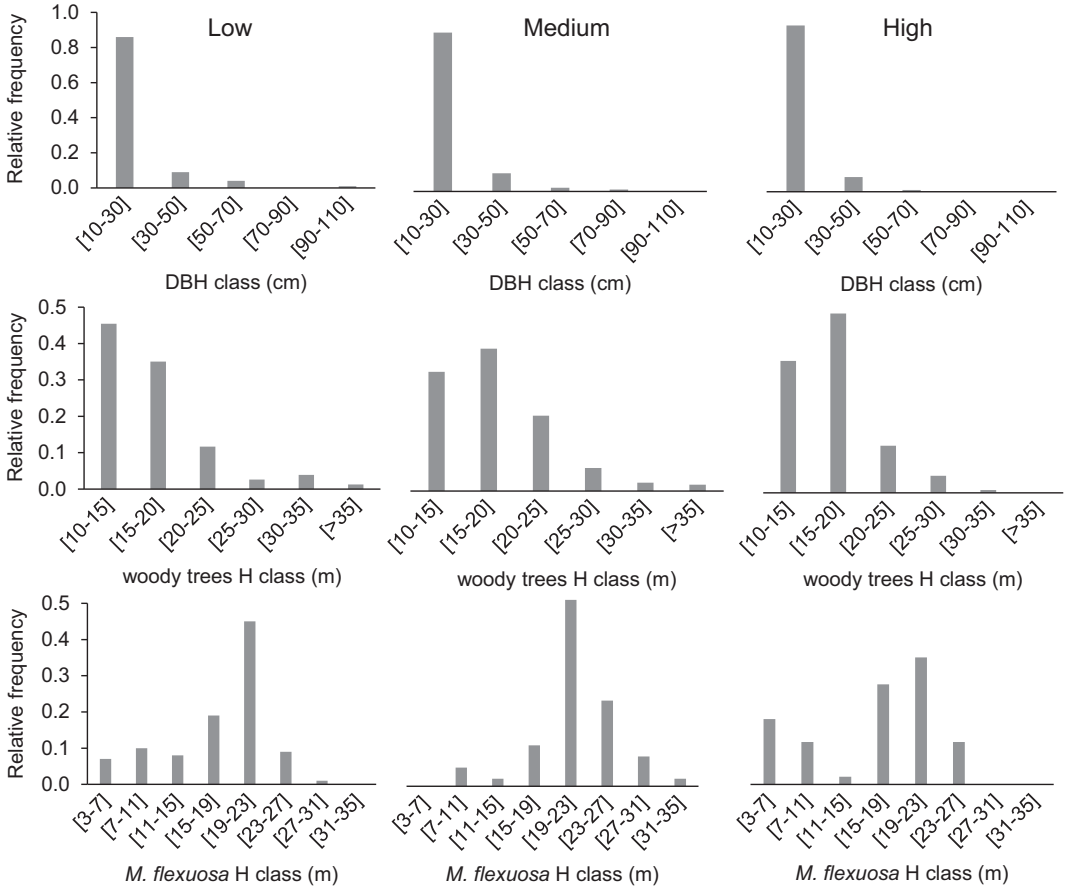

Fig. 3. Relative frequency of diameter at breast height (DBH) (top) and height (H) (middle) of woody trees and H of *M. flexuosa* (bottom) in dense palm swamp plots with different levels of degradation (low, medium, high). The analysis considered woody trees with a DBH > 10 cm and palms with a H > 3 m.

increase is accompanied by a shift in forest composition from palm to woody tree dominated vegetation. The density of *M. flexuosa* palms significantly ($P = 0.0001$) decreased with degradation from 402 ± 30 to 128 ± 4 and 46 ± 13 individuals ha^{-1} in low, medium and high degradation areas, respectively. Most woody trees were small with a DBH <30 cm (Fig. 3 top). Degradation did not seem to have any meaningful effect on the size of woody trees with similar average DBH (19 ± 2, 21 ± 1 and 18 ± 0 in low, medium and high degradation areas) and H (17 ± 1, 18 ± 0 and 17 ± 0 in the same areas) along the degradation gradient (Fig. 3 top and middle). On the contrary, the height of *M. flexuosa* palms was distributed differently according to degradation levels (Fig. 3 bottom). Medium degradation was characterized by a small number (0.07%) of short (<15 m) *M. flexuosa* palms as compared to low (25%) and high (30%) degradation areas. Highly degraded dense PS displayed a much smaller proportion (28%) of *M. flexuosa* with a height >19 m than that in low and medium degradation areas (64 and 61%, respectively). In contrast to total tree density, total biomass C stock was reduced significantly with degradation at a 0.1 level ($P = 0.09$) (Fig. 2 right) with averages of 135.4 ± 4.8, 120.3 ± 5.5 and 112.3 ± 3.1 Mg C ha^{-1} in low, medium and high degradation stands. Medium and high degradation reduced initial biomass C stocks by 11 and 17%, respectively. The contribution of *M. flexuosa* to total C stocks decreased from 72 to 40 and 9% in low, medium and high degradation areas, respectively.

The density of *M. flexuosa* in low degradation areas was much higher than the density reported by Freitas et al. (2006) and Honorio Coronado et al. (2015) (Table 3). Two reasons may explain the discrepancy, first these studies inventoried only palms with a DBH >10 cm and second, degradation may have occurred at the studied sites. On the other hand the data from Horn et al. (2012) which characterize degradation using the male: female ratio of *M. flexuosa* (a ratio of 1 indicating low degradation, a ratio of 10 high degradation) denote higher *M. flexuosa* densities than the ones evaluated in our study no matter the degradation level (Fig. 4). The significant decrease in *M. flexuosa* density with increasing degradation level that we observed is in agreement with the relationship established from the data by Horn et al. (2012). Aboveground biomass in dense PS with low degradation were in the same range as results obtained by Draper et al. (2014) and Honorio Coronado et al. (2015). Dense PS of all degradation levels exhibited a higher total biomass than that evaluated by Freitas et al. (2006) which might be due to the use of a different allometric model for woody trees, in addition to the factors previously mentionned and related to differences in *M. flexuosa* density. Biomass C stocks in dense PS with low degradation are lower than average stocks in Southeast Asian peat swamp forests (207 ± 29 Mg C ha^{-1} with 182 ± 26 located aboveground; Hergoualc'h and Verchot (2011)). Our results suggest that even though the total tree density increases with degradation, the shift in composition from palms to woody trees does not compensate the loss in biomass due to the decrease of *M. flexuosa* palms. Notwithstanding biomass reduction in dense PS are lower than results from studies carried out in Indonesia where degradation following logging activities in peat swamp forests was estimated to reduce initial biomass C stocks by 53% on average (Hergoualc'h and Verchot, 2011); by 30 and 60% for low- and high-intensity logging (Carlson et al., 2012). The implication of degradation on soil C uptakes remains uninvestigated, but it might be of lower impact than that observed in Indonesian peatlands largely affected by drainage. Over there degradation results in both a suppression of peat net GHG uptake in the pristine forest (1.3 ± 5.9 Mg CO_2-eq. ha^{-1} y^{-1}) and in substantial peat emissions in the drained degraded forest (20.9 ± 9.4 Mg CO_2-eq. ha^{-1} y^{-1}) (Drösler et al., 2014; Hergoualc'h and Verchot, 2014) cumulating a total emission rate of 22 ± 11 Mg CO_2-eq. ha^{-1} y^{-1}.

We evaluated degradation impacts on forest structure and biomass using a space-for-time substitution approach. This widely used technique infers past degradation trajectories of dense PS from contemporary spatial patterns (Blois et al., 2013) and therefore assumes that the observed differences are due to degradation and not inherent site differences. We recognize that this approach, if based on a limited knowledge of land use history, may present shortcomings. The biomass inventories indicated that degradation induced a shift in dense PS composition from *M. flexuosa* to woody tree dominated forest. The highly degraded dense PS were located

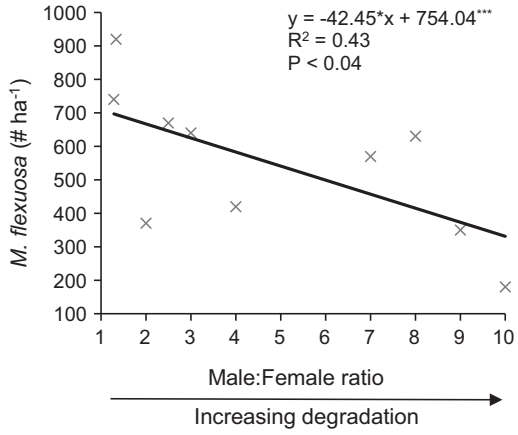

Fig. 4. Relationship between *M. flexuosa* male: female ratio and *M. flexuosa* density in dense palm swamps of the Peruvian Amazon. The data is from Horn et al. (2012) and include palms with a H > 3 m. $^{*}P < 0.05$, $^{**}P < 0.001$.

Table 3
Average ± SE of density of *M. flexuosa*, and aboveground and total biomass (expressed in dry matter and C) of palm swamps (PS) on peat in the Peruvian Amazon according to degradation level and PS type.

Ref	Level of degradation	PS type[d]	# plots	*M. flexuosa* density (# ha^{-1})	AGB (Mg d.m. ha^{-1})	Total biomass (Mg d.m. ha^{-1})	AGB (Mg C ha^{-1})	Total biomass (Mg C ha^{-1})
Here	Low	Dense	2	402 ± 30	224 ± 8	282 ± 10	108 ± 4	135 ± 5
Here	Medium	Dense	2	128 ± 4	200 ± 9	251 ± 11	96 ± 4	120 ± 5
Here	High	Dense	4	46 ± 13	193 ± 5	234 ± 6	93 ± 3	112 ± 3
–[a]	n.a.	Dense	1	280	n.a.	222	n.a.	109
–[a]	n.a.	Mixed	1	72	n.a.	164	n.a.	81
–[b]	n.a.	n.a.	10	n.a.	202 ± 13	n.a.	101 ± 8	n.a.
–[c]	n.a.	Dense	6	208 ± 43	197 ± 19	n.a.	n.a.	n.a.

n.a.: Not available.
[a] Freitas et al. (2006).
[b] Draper et al. (2014).
[c] Honorio Coronado et al. (2015).
[d] Dense indicates a predominance of *M. flexuosa* palms in the stand, mixed depicts an association of *M. flexuosa* with other palms or woody trees.

in between the *Miraflores* and *Aucayacu* sites sampled by Draper et al. (2014), an area classified by the authors as a continuum of PS and pole forest. The potential confusion between highly degraded dense PS and pole forest, both dominated by woody trees, can however be clarified by a series of evidences. First the communities leaving around the degraded area asserted high *M. flexuosa* extraction levels over the past decades. This fact has been documented in the literature (Padoch, 1988; Penn et al., 2008). Theoretically *M. flexuosa* females only are chopped down to collect their fruits. Therefore degraded sites would be expected to have a greater ratio of males than females, as found by Horn et al. (2012). In reality, males are also oftentimes cut down to build tracks to facilitate transportation of the fruits throughout the flooded forest. The proportion of *M. flexuosa* males and females could not be calculated because 30% and 50% of the specimens could not be identified in low-medium and high degradation areas, respectively. Identifying the sex of the palms requires continuous field visits since females do not all flower simultaneously. Notwithstanding the data by Horn et al. (2012) indicate a significant decrease in *M. flexuosa* density along an increase in male: female ratio (Fig. 4) which supports the degradation impacts on dense PS structure observed in this study. Third, the results on structural vari-

Table 4
Area mapped per land cover type. PS designates palm swamps.

Type	Area (ha)
Dense PS with low degradation	11,078
Dense PS with medium degradation	17,250
Dense PS with high degradation	12,771
Dense PS	**41,099**
Mixed PS 1	33,432
Mixed PS 2	16,198
Mixed PS	**49,630**
Total PS	**90,729**
Other land covers	260,595
Total study area	**351,324**

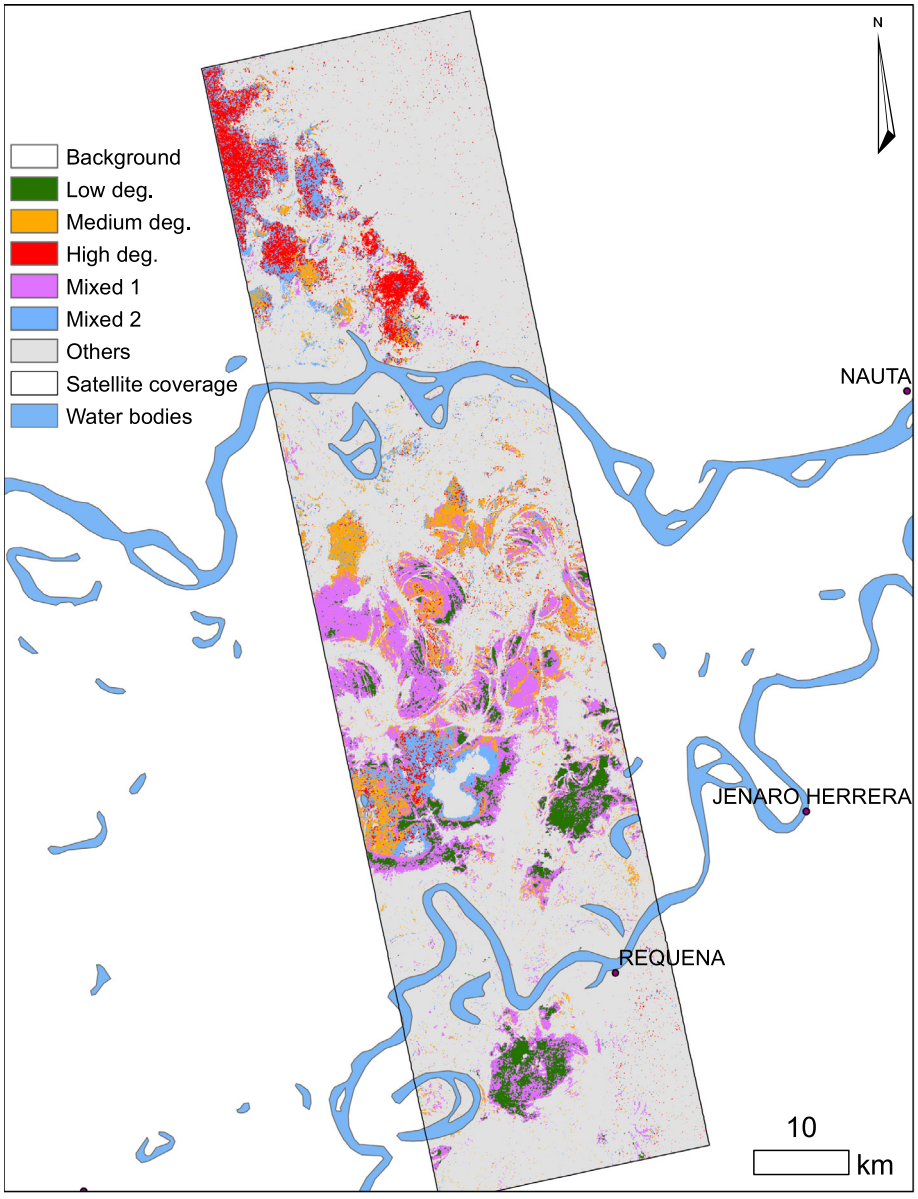

Fig. 5. Land cover classification using a random forest classifier. Low, medium and high deg. refer to dense palm swamps with increasing degradation level. Mixed 1 and 2 designate mixed palm swamps.

ables pointed out a substantial difference in the relative frequency of the height of *M. flexuosa* according to degradation level. In particular, the low proportion of tall palms (H > 19 m) in highly degraded areas, which is uncharacteristic of intact dense PS, suggests human intervention. Finally the height of woody trees in highly degraded sites did not display a distribution (Fig. 3 middle) or an average value (17 m) that concur the description of pole forest given by García-Villacorta et al. (2011), Kelly et al. (2014) and Draper et al. (2014) who all depict pole forest as 5–10 m tall dwarf/low stature forest. These evidences all together support the hypothesis that the shift from palm dominated to woody tree dominated at the investigated sites was a true effect of degradation rather than a natural gradient in vegetation composition.

3.2. Classification of land covers and dense PS degradation

Palm swamps covered 26% of the area mapped, among which 45% corresponded to dense PS (Table 4). Most dense PS were classified as moderately degraded (42%) while areas with low degradation covered the smallest area (27% of dense PS area). The classification map indicates that most of dense PS degradation in the study area is located toward the north, near the point where the *Tigre* and *Marañon* rivers meet (Fig. 5). The biggest patches of dense PS with low degradation are located inside the *Pacaya-Samiria* reserve and toward the south of the image, near the municipality of *Requena*. Results from the Jeffries-Matusita test (Fig. 6) show a good separability between the three degradation categories. Dense PS with low degradation were highly separable from all other categories. Dense PS with medium and high degradation were highly separable from most categories except for *restinga* forests and mixed PS. Jeffries-Matusita values >1 between these categories denote that they are potentially separable if more ground truthing data were collected. Total land cover classification accuracy obtained from the iterative cross validation process in the random forest algorithm was 91% (Fig. 7). The most important variable for land cover classification based on the mean decrease in accuracy and mean decrease in Gini value is the HH ALOS-PALSAR band followed by the third and brightness bands from the tasseled cap transformation (Fig. 8).

Qualitative comparison between our land cover classification map and the one generated by Draper et al. (2014) suggest a close agreement between the two studies. However some small patches located in the north, near the Tigre River and classified here as highly degraded PS were identified as pole forests by Draper et al. In the classification by Draper et al. these areas appear as intricately intermixed with pixels classified as PS, which reflects the continuum between dense PS and pole forests, the latest being located on the thickest, oldest and most ombrotrophic area of the peat deposit as described by the authors. The level of confusion between dense PS highly degraded and pole forests remains to be assessed. On one side, we were not able to include pole forests in our classification because we did not find a land cover fitting that description. On the other side, Draper et al. did not include any category accounting for degradation in dense PS. In the analysis by Draper et al. pole forest was the land cover with the highest commission error (36%) and so the one with the highest probability of over classification. Most of the commission error in that category (30%) corresponded to a misclassification of dense PS as pole forests which is to be expected along a continuum. A more exhaustive field sampling is needed to obtain an accurate characterization of pole forests and their potential confusion with highly degraded PS.

The remote sensing methods and data sources used demonstrated the high potential for discriminating areas of dense PS

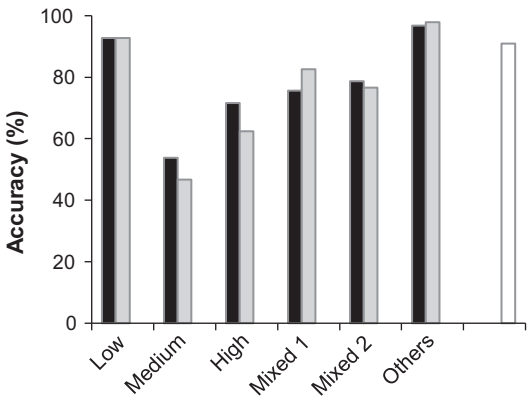

Fig. 7. Land cover classification accuracy. Black, grey, and white fills indicate producer's, user's and overall accuracy.

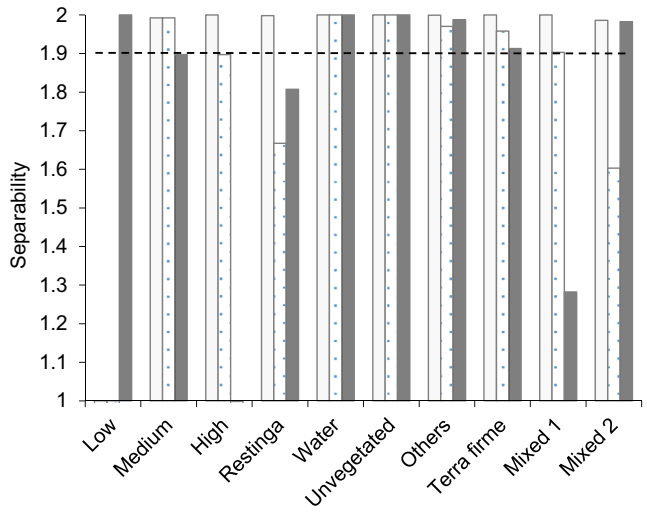

Fig. 6. Spectral separability between dense palm swamps with different levels of degradation (low in light grey, medium with dots and high in dark grey) and other land cover categories based on the Jeffries-Matusita measure. Values below the dashed line indicate that the separability needs to be improved to achieve a satisfactory classification.

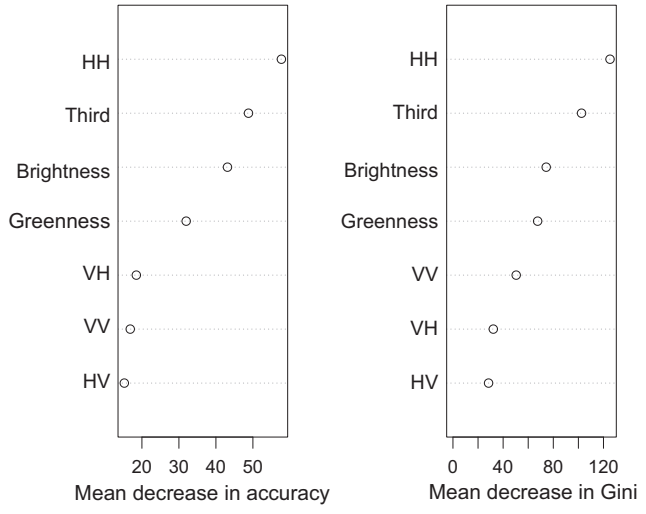

Fig. 8. Variable importance for the land cover classification as measured by the mean decrease in accuracy (left) and the mean decrease in Gini (right). HH, HV, VH and VV are the quad-polarization bands included in the ALOS-PALSAR satellite product. Greenness, brightness and third are the bands resulting from the tasseled cap transformation applied to the Landsat satellite images.

with low degradation from other land covers (Fig. 7). This high classification accuracy combined with the hypothesis that dense PS are reliable indicators of peat soils can support peatland mapping using satellite images from when degradation was still marginal. Furthermore it can particularly facilitate a reliable temporal monitoring of degradation in areas covered by dense PS with low degradation in a reference year. Discrimination between dense PS areas with high and medium degradation and other land covers was moderate but promising (Fig. 7). A larger sampling size would help to assess the intra-class variability in these categories and therefore increase the reliability of the classification accuracy. Given the results of the separability analysis obtained here and the improvement in classification accuracy with increases in sample size obtained in other studies (Rodriguez-Galiano et al., 2012; Shao and Lunetta, 2012), we expect that a larger sample size would increase the classification accuracy. Additional work is also necessary to understand the characteristics in the field that produced differences in the spectral responses between the two mixed PS classes identified in the analysis. The use of satellite images near the peak of the drier season can potentially improve the discrimination of spectral differences in permanently flooded dense PS versus seasonally flooded mixed PS.

Future research might consider assessing the minimum degraded area that can be detected at the spatial resolution of the satellite sources used in the analysis. The use of images from the Sentinel 2 satellites with a higher resolution than images from Landsat in the same optical bands could help identifying small degradation areas. Also forest degradation mapping could potentially be improved by combining the C-band incorporated in the Sentinel 1 satellites with L-band data such as the one used by the ALOS-PALSAR images included in this analysis. This band combination has proved to be useful to map variations in tropical forest structure (Saatchi et al., 2011). Given the local scope of the analysis, further work is needed to assess the feasibility of detecting dense PS forest degradation in a larger scale in Peru and evaluating the transferability of the method to tropical peat swamp forests in other regions.

4. Conclusions

Peruvian peatlands store large amounts of C which are of significant importance in a national and regional context. Despite decades of ongoing degradation little attention has been paid to PS peatlands of the Peruvian Amazon basin. This investigation is a first attempt at mapping and characterizing their degradation by combining remote sensing analysis and ground-based biomass C stock inventories. Our results suggest that dense PS forest degradation is manifested by a change in forest structure from palm dominated to tree dominated vegetation which translates into significant biomass C stock reductions. We also found that remote sensing methods combining both active and passive satellite data are promising for mapping and monitoring dense PS forest degradation regionally. Future research should consider developing additional criteria for identifying degradation, refining biomass loss estimates, measuring peat GHG emissions associated with degradation and evaluating the spatial extent of degradation in the *Mauritia flexuosa* dominated forests of the Amazon. Providing sound and credible estimates of degradation impacts is an essential step before conservation strategies can be planned and adopted. Avoiding deforestation and degradation of Peruvian peatlands is feasible and has a greater chance to succeed through initiatives involving local communities living in these areas. Involving communities would also benefit forest degradation monitoring in such cases of local degradation.

Acknowledgements

This research was made possible through support to CIFOR by USAID (United States Agency for International Development) (Grant Number EEM-G-00-04-00010-00) as part of the CGIAR research programs on Forests, Trees and Agroforestry and Climate Change, Agriculture and Food Security (CCAFS). We are thankful to the field assistants for helping in data collection in difficult conditions and to Tim Baker for a fruitful discussion on tree species in pole forests of the Peruvian Amazon. We are grateful to the anonymous reviewers for their helpful comments that contributed to improve this manuscript.

Appendix A. Supplementary material

Supplementary data associated with this article can be found, in the online version, at http://dx.doi.org/10.1016/j.foreco.2017.03.016.

References

Alvarez, E., Duque, A., Saldarriaga, J., Cabrera, K., de las Salas, G., del Valle, I., Lema, A., Moreno, F., Orrego, S., Rodriquez, L., 2012. Tree above-ground biomass allometries for carbon stock estimation in the natural forests of Colombia. For. Ecol. Manage. 267, 297–308.

ASF. Alaska Satellite Facility (2013) MapReady version 3.1.24. Available at <https://www.asf.alaska.edu/data-tools/mapready/>.

Baccini, A. et al., 2012. Estimated carbon dioxide emissions from tropical deforestation improved by carbon-density maps. Nat. Clim. Change 2, 182–185.

Belgiu, M., Drăgut , L., 2016. Random forest in remote sensing: a review of applications and future directions. ISPRS J. Photogram. Remote Sens. 114, 24–31.

Blois, J.L., Williams, J.W., Fitzpatrick, M.C., Jackson, S.T., Ferrier, S., 2013. Space can substitute for time in predicting climate-change effects on biodiversity. Proc. Natl. Acad. Sci. 110, 9374–9379.

Brady, M.A., 1997. Organic Matter Dynamics of Coastal Peat Deposits in Sumatra, Indonesia Ph D thesis. University of British Columbia.

Breiman, L., 2001. Random forests. Mach. Learn. 45, 5–32.

Carlson, K.M. et al., 2012. Committed carbon emissions, deforestation, and community land conversion from oil palm plantation expansion in West Kalimantan, Indonesia. PNAS 109, 7559–7564.

Chave, J. et al., 2014. Improved allometric models to estimate the aboveground biomass of tropical trees. Glob. Change Biol. 20, 3177–3190.

CFE (Centre for Standardization and Environment), 2011. Measurement and calculation of carbon stocks – Field measurement for estimating forest carbon stocks (ground based forest carbon accounting). Ministry of forestry, Indonesia.

Chander, G., Markham, B.L., Helder, D.L., 2009. Summary of current radiometric calibration coefficients for Landsat MSS, TM, ETM+, and EO-1 ALI sensors. Remote Sens. Environ. 113, 893–903.

Crist, E., Cicone, R., 1984. Application of the tasseled cap concept to simulated thematic mapper data. Photogram. Eng. Remote Sens. 50, 343–352.

Dargie, G.C., Lewis, S.L., Lawson, I.T., Mitchard, E.T.A., Page, S.E., Bocko, Y.E., Ifo, S.A., 2017. Age, extent and carbon storage of the central Congo Basin peatland complex. Nature 542, 86–90.

Draper, F.C. et al., 2014. The distribution and amount of carbon in the largest peatland complex in Amazonia. Environ. Res. Lett. 9. http://dx.doi.org/10.1088/1748-9326/1089/1012/124017.

Drösler, M. et al., 2014. Chapter 2 Drained inland organic soils. In: Hiraishi, T., Krug, T., Tanabe, K., Srivastava, N., Jamsranjav, B., Fukuda, M., Troxler, T. (Eds.), 2013 Supplement to the 2006 guidelines for national greenhouse gas inventories: Wetlands. IPCC, Switzerland.

Earth explorer, 2013. <http://earthexplorer.usgs.gov/>.

Englhart, S., Jubanski, J., Siegert, F., 2013. Quantifying dynamics in tropical peat swamp forest biomass with multi-temporal LiDAR datasets. Remote Sens. 5, 2368–2388.

Fernández-Delgado, M., Cernadas, E., Barro, S., Amorim, D., 2014. Do we need hundreds of classifiers to solve real world classification problems? J. Mach. Learn. Res. 15, 3133–3181.

Freitas, L., Otárola, E., del Castillo, D., Linares, C., Martínez, P., Malca, G.A., 2006. Servicios ambientales de almacenamiento y secuestro de carbono del ecosistema aguajal en la reserva nacional Pacaya Samiria, Loreto - Perú. Documento técnico n°29. Iquitos, Perú.

García-Villacorta, R., Huamantupa, I., Cordero, Z., Pitman, N., Vriesendorp, C., 2011. Flora and vegetation. In: Pitman, N. et al. (Eds.), Perú: Yaguas-Cotuhé. Rapid Biological and Social Inventories Report 23. The Field Museum, pp. 86–97.

Gaveau, D.L.A. et al., 2014. Major atmospheric emissions from peat fires in Southeast Asia during non-drought years: evidence from the 2013 Sumatran fires. Nat. Sci. Rep. 4. http://dx.doi.org/10.1038/srep06112.

GLOVIS, 2013. <http://glovis.usgs.gov/>.
González-B, V., Rial, A., 2013. Terminología y tipos de agrupación de Mauritia flexuosa según el paisaje. Capítulo 4. In: Lasso CA, Rial A, González-B V (Eds.), VII. Morichales y canangunchales de la Orinoquia y Amazonia: Colombia – Venezuela. Parte I. Instituto de Investigación de Recursos Biológicos Alexander, Bogotá, D. C., Colombia, pp. 75–83.
Gonzales Davila, E., Noriega Pereira, R., Llanos Dulanto, D., Paredes Zumaeta, J., Paredes Mori, J., 2007. Plan de manejo de Mauritia flexuosa "aguaje" en la comunidad veinte de enero, cuenca Yanayacu-Pucate- Reserva Nacional Pacaya Samiria 2005–2009. ProNaturaleza, USAID, TNC.
Goodman, R.C., Phillips, O.L., del Castillo, Torres.D., Freitas, L., Tapia Cortese, S., Monteagudo, A., Baker, T.R., 2013. Amazon palm biomass and allometry. For. Ecol. Manage. 310, 994–1004.
Gutiérrez-Vélez, V.H., DeFries, R., 2013. Annual multi-resolution detection of land cover conversion to oil palm in the Peruvian Amazon. Remote Sens. Environ. 129, 154–167.
Hergoualc'h, K., Verchot, L.V., 2011. Stocks and fluxes of carbon associated with land-use change in Southeast Asian tropical peatlands: a review. Glob. Biochem. Cycl. 25, GB2001. http://dx.doi.org/10.1029/2009GB003718.
Hergoualc'h, K., Verchot, L.V., 2014. Greenhouse gas emission factors for land use and land-use change in Southeast Asian peatlands. Mitig. Adapt. Strateg. Glob. Change 19, 789–807.
Honorio Coronado, E.N., Vega Arenas, J.E., Corrales Medina, M.N., 2015. Diversidad, estructura y carbono de los bosques alluviales del Noreste Perunao. Folia Amazónica 24, 55–70.
Horn, C.M., Gilmore, M.P., Endress, B.A., 2012. Ecological and socio-economic factors influencing aguaje (Mauritia flexuosa) resource management in two indigenous communities in the Peruvian Amazon. For. Ecol. Manage. 267, 93–103.
Householder, J.E., Janovec, J.P., Tobler, M.W., Page, S., Lähteenoja, O., 2012. Peatlands of the Madre de Dios River of Peru: distribution, geomorphology, and habitat diversity. Wetlands. http://dx.doi.org/10.1007/s13157-13012-10271-13152.
IIAP, 2004. Diversidad de la vegetación de la Amazonía Peruana expresada en un mosaico de imagenes de satélite. Documento técnico N°12 Iquitos, Perú. Proyecto diversidad biológica de la Amazonía Peruana BIODAMAZ (Perú-Finlandia).
Infostat, 2014. Di Rienzo JA, Casanoves F, Balzarini MG, Gonzalez L, Tablada M, Robledo CW InfoStat Group, Facultad de Ciencias Agropecuarias, Universidad Nacional de Córdoba, Argentina. <http://www.infostat.com.ar>.
IPCC, 2006. 2006 IPCC Guidelines for National Greenhouse Gas Inventories. Institute for Global Environmental Strategies (IGES), Hayama, Japan.
ITT Visual Information Solutions, 2013. ENVI version 5.0.2.
Jaenicke, J., Rieley, J.O., Mott, C., Kimman, P., Siegert, F., 2008. Determination of the amount of carbon stored in Indonesian peatlands. Geoderma 147, 151–158.
Janovec, J. et al., 2013. Evaluación de los actuales impactos y amenazas inminentes en aguajales y cochas de Madre de dios, Perú. WWF, Lima, Peru.
Jensen, J., 2016. Introductory Digital Image Processing: A Remote Sensing Perspective. Pearson Education Inc., Boston, p. 623.
Kahn, F., Mejia, K., 1990. Palm communities in wetland forest ecosystems of Peruvian Amazonia. For. Ecol. Manage. 33 (44), 169–179.
Kelly, T.J., Baird, A.J., Roucoux, K.H., Baker, T.R., Honorio Coronado, E.N., Ríos, M., Lawson, I.T., 2014. The high hydraulic conductivity of three wooded tropical peat swamps in northeast Peru: measurements and implications for hydrological function. Hydrol. Process. 28, 3373–3387.
Koh, L.P., Miettinen, J., Liew, S.C., Ghazoul, J., 2011. Remotely sensed evidence of tropical peatland conversion to oil palm. Proc. Natl. Acad. Sci. 108, 5127–5132.
Lähteenoja, O., Page, S., 2011. High diversity of tropical peatland ecosystem types in the Pastaza-Marañón basin, Peruvian Amazonia. J. Geophys. Res. 116. http://dx.doi.org/10.1029/2010JG001508.
Lähteenoja, O., Rojas Reátegui, Y., Räsänen, M., Del Castillo, Torres.D., Oinonen, M., Page, S., 2012. The large Amazonian peatland carbon sink in the subsiding Pastaza-Marañón foreland basin, Peru. Glob. Change Biol. 18, 164–178.
Lähteenoja, O., Roucoux, K.H., 2010. Inception, history and development of peatlands in the Amazon Basin. PAGES News 18, 27–29.
Lähteenoja, O., Ruokolainen, K., Schulman, L., Alvarez, J., 2009a. Amazonian floodplains harbour minerotrophic and ombrotrophic peatlands. Catena, 140–145.
Lähteenoja, O., Ruokolainen, K., Schulman, L., Oinonen, M., 2009b. Amazonian peatlands: an ignored C sink and potential source. Glob. Change Biol. 15, 2311–2320.
Laumonier, Y., 1997. The Vegetation and Physiography of Sumatra. Geobotany, vol. 22. Kluwer Academic Publishers, Dordrecht, The Netherlands.
Lehner, B., Verdin, K., Jaris, A., 2006. HydroSHEDS (Hydrological data and maps based on shuttle elevation derivates at multiple scales. World Wildlife fund US, Washington, DC. Available at: <http://hydrosheds.cr.usgs.gov>.
Manuri, S., Brack, C., Nugroho, N.P., Hergoualc'h, K., Novita, N., Dotzauer, H., Verchot, L., Septiadi, C.A.P., Widyasari, E., 2014. Tree biomass equations for tropical peat swamp forest ecosystems in Indonesia. For. Ecol. Manage. 334, 241–253.
Miettinen, J., Liew, S.C., 2010a. Degradation and development of peatlands in Peninsular Malaysia and in the islands of Sumatra and Borneo since 1990. Land Degrad. Dev. 21, 285–296.
Miettinen, J., Liew, S.C., 2010b. Status of peatland degradation and development in Sumatra and Kalimantan. Ambio 39, 394–401.
Miettinen, J., Hooijer, A., Wang, J., Shi, C., Liew, S.C., 2012. Peatland degradation and conversion sequences and interrelations in Sumatra. Reg. Environ. Change 12, 729–737.
Miettinen, J., Stibig, H.-J., Achard, F., 2014. Remote sensing of forest degradation in Southeast Asia – aiming for a regional view through 5–30 m satellite data. Glob. Ecol. Conserv. 2, 24–36.
Mokany, K., Raison, R.J., Prokushkin, A.S., 2006. Critical analysis of root: shoot ratios in terrestrial biomes. Glob. Change Biol. 12, 84–96.
Murdiyarso, D., Donato, D., Kauffman, J.B., Kurnianto, S., Stidham, M., Kanninen, M., 2009. Carbon storage in mangrove and peatland ecosystems. A preliminary account from plots in Indonesia. CIFOR Working Paper 48, 35 p.
Nyoungui, A.N., Tonye, E., Akono, A., 2002. Evaluation of speckle filtering and texture analysis methods for land cover classification from SAR images. Int. J. Remote Sens. 23, 1895–1925.
Padoch, C., 1988. Aguaje (*Mauritia flexuosa* L.f.) in the economy of Iquitos, Peru. Adv. Econ. Bot. 6, 214–224.
Page, S.E., Rieley, J.O., Banks, C.J., 2011. Global and regional importance of the tropical peatland carbon pool. Glob. Change Biol. 17, 798–818.
PASCO, 2013. <http://en.alos-pasco.com/offer/>.
Pearson, T.R.H., Brown, S., Murray, L., Sidman, G., 2017. Greenhouse gas emissions from tropical forest degradation: an underestimated source. Carbon Balance Manage. 12. http://dx.doi.org/10.1186/s13021-13017-10072-13022.
Penn, J., van Sledright, M., Bertiz Torres, G., Guerra Soplín, E., 2008. Los aguajales y sus condiciones en el Río Tahuayo: Aportes para el Plan Maestro del Área de Conservación Regional ComunalTamshiyacu-Tahuayo (ACRCTT). Programa de conservación, gestión y uso sostenible de la diversidad biológica en la región Loreto (PROCREL), Iquitos, Perú.
Penn, J.W., 2008. Non-timber forest products in Peruvian Amazonia: changing patterns of economic exploitation. Focus Geogr. 51, 18–25.
R Core Team, 2013. R: A Language and Environment for Statistical Computing. R Foundation for Statistical Computing, Vienna, Austria. <http://www.R-project.org/>.
Räsänen, M., Neller, R., Salo, J., Jungner, H., 1992. Recent and ancient fluvial deposition systems in the Amazonian foreland basin, Peru. Geol. Mag. 129, 293–306.
Richards, J.A., 1999. Remote Sensing Digital Image Analysis. Springer-Verlag, Berlin.
Rodriguez-Galiano, V.F., Ghimire, B., Rogan, J., Chica-Olmo, M., Rigol-Sanchez, J.P., 2012. An assessment of the effectiveness of a random forest classifier for land-cover classification. ISPRS J. Photogram. Remote Sens. 67, 93–104.
Román-Cuesta, R.M. et al., 2011. Implications of fires on carbon budgets in Andean cloud montane forest: the importance of peat soils and tree resprouting. For. Ecol. Manage. 261, 1987–1997.
Saatchi, S., Marlier, M., Chazdon, R.L., Clark, D.B., Russell, A.E., 2011. Impact of spatial variability of tropical forest structure on radar estimation of aboveground biomass. Remote Sens. Environ. 115, 2836–2849.
Shao, Y., Lunetta, R.S., 2012. Comparison of support vector machine, neural network, and CART algorithms for the land-cover classification using limited training data points. ISPRS J. Photogram. Remote Sens. 70, 78–87.
Shimabukuro, Y.E., Beuchle, R., Grecchi, R.C., Achard, F., 2014. Assessment of forest degradation in Brazilian Amazon due to selective logging and fires using time series of fraction images derived from Landsat ETM+ images. Remote Sens. Lett. 5, 773–782.
Sierra, C.A. et al., 2007. Total carbon stocks in a tropical forest landscape of the Porce region, Colombia. For. Ecol. Manage. 243, 299–309.
van der Werf, G.R. et al., 2008. Climate regulation of fire emissions and deforestation in equatorial Asia. Proc. Natl. Acad. Sci. U.S.A. 105, 20350–20355.
Weiskittel, A.R., Hann, D.W., Kershaw, J.A., Vanclay, J.K., 2011. Forest Growth and Yield Modeling. Wiley-Blackwell, Chichester, West Sussex, UK.
Yuan, D., Elvidge, C.D., 1996. Comparison of relative radiometric normalization techniques. ISPRS J. Photogramm. Remote Sens. 51, 117–126.
Yu, Z., Loisel, J., Brosseau, D.P., Beilman, D.W., Hunt, S.J., 2010. Global peatland dynamics since the Last Glacial Maximum. Geophys. Res. Lett. 37. http://dx.doi.org/10.1029/2010GL043584.
Zianis, D., 2008. Predicting mean aboveground forest biomass and its associated variance. For. Ecol. Manage. 256, 1400–1407.